

Comparison of Intensity- and Jacobian-Based Estimates of Lung Regional Ventilation

Kai Ding¹, Kunlin Cao², Ryan E. Amelon¹, Gary E. Christensen²
Madhavan L. Raghavan¹, and Joseph M. Reinhardt^{1*}

¹ Department of Biomedical Engineering

² Department of Electrical and Computer Engineering
The University of Iowa, Iowa City, IA 52242

{kai-ding, kunlin-cao, ryan-amelon, gary-christensen,
ml-raghavan, joe-reinhardt}@uiowa.edu

Abstract. Regional ventilation is the measurement of pulmonary function on a local, or regional level. The measurement of pulmonary function may be useful as a planning tool during radiation therapy (RT) planning, may be useful for tracking the progression of toxicity to nearby normal tissue during RT and can be used to evaluate the effectiveness of a treatment post-therapy. In this paper, we show that an intensity-based regional ventilation measure can be derived from a Jacobian-based measure by relaxing the assumption that there is no tissue volume change. We compare intensity-based and Jacobian-based measures of regional ventilation to xenon-CT (Xe-CT) measures of specific ventilation. The results show that the Jacobian-based measure correlates better (average $r^2 = 0.80$) with Xe-CT-based measures of specific ventilation than the intensity-based measure (average $r^2 = 0.54$). The difference between the intensity-based measure and the Jacobian-based measure of regional ventilation is linearly related to the tissue volume difference between scans (average $r^2 = 0.86$).

1 Introduction

Regional ventilation is the term used to characterize the volume of air per unit time that enters or exits the lung on a local, or regional, level. Since the primary function of the lung is gas exchange, ventilation can be interpreted as an index of lung function. Injury and disease processes can alter lung function on a global and/or a local level. Recent advances in multi-detector-row CT (MDCT), 4DCT respiratory gating methods, and image processing techniques enable us to study pulmonary function at the regional level with high resolution anatomical information compared to other methods. MDCT can be used to acquire multiple static breath-hold CT images of the lung taken at different lung volumes, or 4DCT images of the lung reconstructed at different respiratory phases with proper respiratory control. Image registration can be applied to this data to

* J. M. Reinhardt is shareholder in VIDA Diagnostics, Inc.

estimate a deformation field that transforms the lung from one volume configuration to the other. This deformation field can be analyzed to estimate local lung tissue expansion, calculate voxel-by-voxel intensity change, ventilation, and make biomechanical measurements [1–5].

An important emerging application of these methods is the detection of pulmonary function change in subjects undergoing radiation therapy (RT) for lung cancer. During RT, treatment is commonly limited to sub-therapeutic doses due to unintended toxicity to normal lung tissue. Reducing the frequency of occurrence and magnitude of normal lung function loss may benefit from treatment plans that incorporate relationships between regional and functional based lung information and the radiation dose. Measurement of pulmonary function may be useful as a planning tool during RT planning, may be useful for tracking the progression of toxicity to nearby normal tissue during RT, and can be used to evaluate the effectiveness of a treatment post-therapy [6, 7].

The physiologic significance of the registration-based measures of respiratory function can be established by comparing to more conventional measurements, such as nuclear medicine or contrast wash-in/wash-out studies with CT or MR. Xenon-enhanced CT (Xe-CT) measures regional ventilation by observing the gas wash-in and wash-out rate on serial CT images [8]. Xe-CT imaging has the advantage of high temporal resolution and anatomical information. Although it comes along with limited axial coverage, it can be used to compare with registration-based measures of regional lung function in animal studies for validation purpose.

This paper describes two measures to estimate regional ventilation from image registration of CT images: the intensity based and the Jacobian based measures. We show that the intensity based regional ventilation measure can be derived from Jacobian based measure by making the assumption that there is no tissue volume change. They are evaluated by comparison with Xe-CT estimated ventilation. These results may provide insight into which measures may best estimate regional ventilation using image registration of respiratory-gated CT images.

2 Material and methods

2.1 Data Acquisition

Three sheep were anesthetized and mechanically ventilated during experiments. The 4DCT images were acquired with the animals in the supine position using the dynamic imaging protocol and images were reconstructed retrospectively. The 0% (EE) and 100% (EI) inspiration phases were used for ventilation measurements. Twelve contiguous axial locations and approximately 45 breaths for the Xe-CT studies were selected from the whole lung volumetric scan performed near end-expiration (EE₀ to EE₄₄). The animal was not moved between scans. The respiratory rate (RR) for three animals ranges from 15 to 18 breaths per minute. Both the 4DCT and the Xe-CT images were reconstructed using a ma-

trix of 512 by 512 pixels. The in-plane pixel spacing is approximately $0.5 \text{ mm} \times 0.5 \text{ mm}$.

2.2 Image Registration

The tissue volume and vesselness measure preserving nonrigid registration (TVP) algorithm is used to estimate transforms EI to EE and EE_0 to EE. The algorithm minimizes the sum of squared tissue volume difference (SSTVD) [9] and vesselness measure difference (SSVMD), utilizing the rich image intensity information and natural anatomic landmarks provided by the vessels. This method has been shown to be effective at registering across lung CT images with high accuracy [10, 11].

Let I_1 and I_2 represent two 3D image volumes to be registered. The vector \mathbf{x} defines the voxel coordinate within an image. The algorithm find the optimal transformation \mathbf{h} that maps the template image I_1 to the target image I_2 by minimizing the cost function

$$C_{\text{TOTAL}} = \rho \int_{\Omega} [V_2(\mathbf{x}) - V_1(\mathbf{h}(\mathbf{x}))]^2 d\mathbf{x} + \chi \int_{\Omega} [F_2(\mathbf{x}) - F_1(\mathbf{h}(\mathbf{x}))]^2 d\mathbf{x}. \quad (1)$$

where Ω is the union domain of the images I_1 and I_2 . The first integral of the cost function defines the SSTVD cost and the second integral of the cost function defines the SSVMD cost.

The SSTVD cost assumes that the measured Hounsfield units (HU) in the lung CT images is a function of tissue and air content. Following the findings by Hoffman et. al [12], from the CT value of a given voxel, the tissue volume can be estimated as

$$V(\mathbf{x}) = \nu(\mathbf{x}) \frac{I(\mathbf{x}) - HU_{air}}{HU_{tissue} - HU_{air}} = \nu(\mathbf{x})\beta(I(\mathbf{x})), \quad (2)$$

and the air volume can be estimated as

$$V'(\mathbf{x}) = \nu(\mathbf{x}) \frac{HU_{tissue} - I(\mathbf{x})}{HU_{tissue} - HU_{air}} = \nu(\mathbf{x})\alpha(I(\mathbf{x})), \quad (3)$$

where $\nu(\mathbf{x})$ denotes the volume of voxel \mathbf{x} and $I(\mathbf{x})$ is the intensity of a voxel at position \mathbf{x} . HU_{air} and HU_{tissue} refer to the intensity of air and tissue, respectively. In this work, we assume that air is -1000 HU and tissue is 0 HU. $\alpha(I(\mathbf{x}))$ and $\beta(I(\mathbf{x}))$ are introduced for notational simplicity, and $\alpha(I(\mathbf{x})) + \beta(I(\mathbf{x})) = 1$.

Given (2), we can then define the SSTVD cost:

$$C_{\text{SSTVD}} = \int_{\Omega} [\nu_2(\mathbf{x})\beta(I_2(\mathbf{x})) - \nu_1(\mathbf{h}(\mathbf{x}))\beta(I_1(\mathbf{h}(\mathbf{x})))]^2 d\mathbf{x} \quad (4)$$

With the warping function $\mathbf{h}(\mathbf{x})$, $I_1(\mathbf{h}(\mathbf{x}))$ can be interpolated from the template image. $\nu_1(\mathbf{h}(\mathbf{x}))$ can be calculated from the Jacobian $J(\mathbf{x})$ of the deformation as $\nu_1(\mathbf{h}(\mathbf{x})) = J(\mathbf{x})\nu_2(\mathbf{x})$.

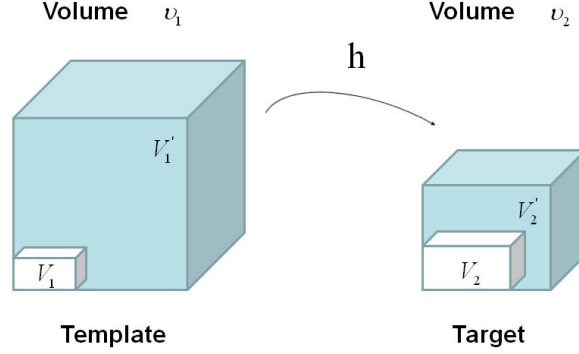


Fig. 1. Example of a given voxel under deformation $\mathbf{h}(\mathbf{x})$ from template image to target image. V_1 and V_2 are tissue volumes. V'_1 and V'_2 are air volumes.

Figure 1 shows an example of a given cube under deformation \mathbf{h} from template image to target image. The total cube volumes are ν_1 and ν_2 . The total cube volume can be decomposed into the tissue volume and air volume based on their individual intensity. The small white volume inside the cube represents the tissue volume V_1 and V_2 . The air volume is represented by V'_1 and V'_2 in blue. As the ratio of air to tissue decreases, the CT intensity of a voxel increases. The intensities of the cubes in the template image and the target image are I_1 and I_2 and are a function of the ratio of air to tissue content of the cube.

As the blood vessels branch to small diameters, the raw grayscale information from vessel voxels provide almost no contribution to guide the intensity-based registration. To better utilize the information of blood vessel locations, we use the vesselness measure (VM) based on the eigenvalues of the Hessian matrix of image intensity. Frangi's vesselness function [13] is defined as

$$F(\lambda) = \begin{cases} (1 - e^{-\frac{R_A^2}{2\alpha^2}}) \cdot e^{-\frac{R_B^2}{2\beta^2}} \cdot (1 - e^{-\frac{S^2}{2\gamma^2}}) & \text{if } \lambda_2 < 0 \text{ and } \lambda_3 < 0 \\ 0 & \text{otherwise} \end{cases} \quad (5)$$

with

$$R_A = \frac{|\lambda_2|}{|\lambda_3|}, \quad R_B = \frac{|\lambda_1|}{\sqrt{|\lambda_2\lambda_3|}}, \quad S = \sqrt{\lambda_1^2 + \lambda_2^2 + \lambda_3^2}, \quad (6)$$

where R_A distinguishes between plate-like and tubular structures, R_B accounts for the deviation from a blob-like structure, and S differentiates between tubular structure and noise. α , β , γ control the sensitivity of the vesselness measure. The vesselness measure is rescaled to $[0, 1]$ and can be considered as a probability-like estimate of vesselness features. For this study, $\alpha = 0.5$, $\beta = 0.5$, and $\gamma = 5$. The transformation $\mathbf{h}(\mathbf{x})$ is a cubic B-splines transform. Note that the Jacobian value must be positive here, which can be achieved by using displacement constraints on the control nodes [14]. The total cost in equation 1 is optimized using a limited-memory, quasi-Newton minimization method with bounds (L-BFGS-B) algorithm.

2.3 Regional Ventilation Measures from Image Registration

After we obtain the optimal warping function, we can calculate the regional ventilation, which is equal to the difference in local air volume change per unit time. Therefore, the specific ventilation (SV) is equal to specific air volume change per unit time.

Specific air volume change by corrected Jacobian (SACJ): Applying the same assumptions (2) and (3) used in the SSTVD cost function, we have

$$SACJ = \frac{V_1'(\mathbf{h}(\mathbf{x})) - V_2'(\mathbf{x})}{V_2'(\mathbf{x})} \quad (7)$$

$$= \frac{\nu_1(\mathbf{h}(\mathbf{x}))\alpha(I_1(\mathbf{h}(\mathbf{x})))}{\nu_2(\mathbf{x})\alpha(I_2(\mathbf{x}))} - 1 \quad (8)$$

Given a warping function $\mathbf{h}(\mathbf{x})$, $I_1(\mathbf{h}(\mathbf{x}))$ can be interpolated from the template image. $\nu_1(\mathbf{h}(\mathbf{x}))$ can be calculated from the Jacobian $J(\mathbf{x})$ of the deformation as $\nu_1(\mathbf{h}(\mathbf{x})) = J(\mathbf{x})\nu_2(\mathbf{x})$. Therefore, the specific air volume change is then

$$SACJ = J(\mathbf{x}) \frac{\alpha(I_1(\mathbf{h}(\mathbf{x})))}{\alpha(I_2(\mathbf{x}))} - 1 \quad (9)$$

$$= J(\mathbf{x}) \frac{HU_{tissue} - I_1(\mathbf{h}(\mathbf{x}))}{HU_{tissue} - I_2(\mathbf{x})} - 1 \quad (10)$$

$$= J(\mathbf{x}) \frac{I_1(\mathbf{h}(\mathbf{x}))}{I_2(\mathbf{x})} - 1. \quad (11)$$

The correction factor $\frac{I_1(\mathbf{h}(\mathbf{x}))}{I_2(\mathbf{x})}$ above depends on the voxel intensity.

Specific air volume change by intensity (SAI): The intensity based measure of regional air volume change SAI can be derived from the SACJ. Now we introduce another assumption that the tissue volume is preserved, or equivalently, that the tissue volume difference $\Delta V(\mathbf{x}) = V_1(\mathbf{h}(\mathbf{x})) - V_2(\mathbf{x}) = 0$. Under this assumption, $V_1(\mathbf{h}(\mathbf{x})) = V_2(\mathbf{x})$ and we have

$$\nu_1(\mathbf{h}(\mathbf{x}))\beta(I_1(\mathbf{h}(\mathbf{x}))) = \nu_2(\mathbf{x})\beta(I_2(\mathbf{x})), \quad (12)$$

and

$$\nu_1(\mathbf{h}(\mathbf{x})) = \nu_2(\mathbf{x}) \frac{\beta(I_2(\mathbf{x}))}{\beta(I_1(\mathbf{h}(\mathbf{x})))}, \quad (13)$$

Since $\nu_1(\mathbf{h}(\mathbf{x})) = J(\mathbf{x})\nu_2(\mathbf{x})$, with above equation, we have

$$J(\mathbf{x}) = \frac{\beta(I_2(\mathbf{x}))}{\beta(I_1(\mathbf{h}(\mathbf{x})))} \quad (14)$$

$$= \frac{I_2(\mathbf{x}) - HU_{air}}{I_1(\mathbf{h}(\mathbf{x})) - HU_{air}}. \quad (15)$$

Substituting the above equation into equation 10 with assumption that air is -1000 HU and tissue is 0 HU, then

$$SAI = 1000 \frac{I_1(\mathbf{h}(\mathbf{x})) - I_2(\mathbf{x})}{I_2(\mathbf{x})(I_1(\mathbf{h}(\mathbf{x})) + 1000)} \quad (16)$$

which is exactly the equation as described in Simon [15], Guerrero et al. [1] and Fuld et al. [16].

Difference of specific air volume change (DSA) and difference of tissue volume (DT): To investigate the relationship between the measurements of specific air volume changes and the tissue volume change, we also measure the difference between equation (11) and equation (16) by comparing the difference of specific air volume change (DSA) between SACJ and SAI, and the difference of tissue volume (DT) as:

$$DSA = SACJ - SAI \quad (17)$$

$$DT = V_1(\mathbf{h}(\mathbf{x})) - V_2(\mathbf{x}) \quad (18)$$

$$= J(\mathbf{x})\nu_2(\mathbf{x})\beta(I_1(\mathbf{h}(\mathbf{x}))) - \nu_2(\mathbf{x})\beta(I_2(\mathbf{x})) \quad (19)$$

$$= \nu_2(\mathbf{x}) \frac{J(\mathbf{x})(I_1(\mathbf{h}(\mathbf{x})) - HU_{air}) - (I_2(\mathbf{x}) - HU_{air})}{HU_{tissue} - HU_{air}} \quad (20)$$

$$= \nu_2(\mathbf{x}) \frac{J(\mathbf{x})(I_1(\mathbf{h}(\mathbf{x})) + 1000) - (I_2(\mathbf{x}) + 1000)}{1000}. \quad (21)$$

In this study, the absolute values of DT and DSA are used in analysis.

2.4 Compare Registration Regional Ventilation Measures to Xe-CT Estimated Ventilation

The Xe-CT estimate of SV is computed in the coordinates of the EE_0 using Pulmonary Analysis Software Suite 11.0 (PASS) [17] at the original image size of $0.5 \text{ mm} \times 0.5 \text{ mm} \times 2.4 \text{ mm}$ voxels. Overlapping 1×8 regions of interest (ROI) are defined in the lung region on each 2D slice. All the images including the EE, EI, EE_0 and SV map are then resampled to a voxel size of $1 \text{ mm} \times 1 \text{ mm} \times 1 \text{ mm}$. After preprocessing, EI is registered to EE using the TVP for measuring the regional ventilation from these two phases in a 4DCT scan. The resulting transformation is used to estimate the SACJ and SAI. Then EE_0 is registered to EE using TVP as well to map the SV to the same coordinate system as that of the SACJ and SAI. A semi-automatic landmark system is used for landmark detection and annotation [18]. For each animal, after 200 anatomic landmarks are identified in the EE, the observer marks the locations of the voxels corresponding to the anatomic locations of the landmarks in the EI. For each landmark, the actual landmark position is compared to the registration-derived estimate of landmark position and the error is calculated. To compare

the regional ventilation measures, the corresponding region of Xe-CT image EE_0 in the EE is divided into about 100 cubes with size of $20 \text{ mm} \times 20 \text{ mm} \times 20 \text{ mm}$. We compare the average regional ventilation measures (SACJ and SAI) to the corresponding average SV measurement from Xe-CT images within each cube. The correlation coefficients between any two estimates (SACJ-SV or SAI-SV) are calculated by linear regression. To compare two correlation coefficients, the Fisher Z-transform of the r values is used and the level of significance is determined [19]. The relationship between the specific air volume change and difference of tissue volume is also studied in three animals by linear regression analysis.

3 Results

3.1 Registration Accuracy

Approximately 200 automatic identified landmarks within the lungs are used to compute the registration accuracy. The landmarks are uniformly distributed in the lung regions. Figure 2 shows an example of the distribution of the landmarks in on animal for both the EE and EI images. The coordinate of each landmark location is recorded for each image data set before and after registration. For all three animals, before registration, the average landmark distance is 6.6 mm with minimum 1.0 mm, maximum 14.6 mm and stand deviation 2.42 mm. After registration, the average landmark distance is 0.4 mm with minimum 0.1 mm, maximum 1.6 mm and stand deviation 0.29 mm.

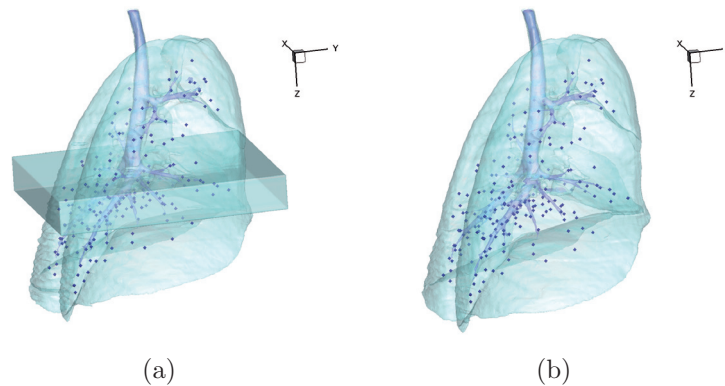


Fig. 2. 3D view of the landmarks in: (a) EE with EE_0 and (b) EI. The dark region below the carina in (a) is the EE_0 and the spheres are the automatically defined landmarks.

3.2 Registration Estimated Ventilation Compared to Xe-CT Estimated Ventilation

Figure 3(a) shows an example of the color-coded cubes of the regions where we average the registration estimated ventilation measures and the Xe-CT estimated SV and compare them. For each animal, the corresponding Xe-CT regions in the EE are divided into about 100 cubes. Figure 3(b) is the Xe-CT estimate of SV. Figure 3(c), (d) are the corresponding registration ventilation measures SACJ and SAI. The regions with edema are excluded from the comparison. Figure 3(b) to (d) all show noticeable similar gradient in the ventral-dorsal direction. Notice that the color scales are different in each map and are set according to their ranges in Fig. 4.

Figure 4 shows the scatter plots between the registration ventilation measures and the Xe-CT ventilation SV with linear regression in all three animals. The SACJ column shows the stronger correlation (average $r^2 = 0.80$) than the intensity based measure SAI (average $r^2 = 0.54$) with the SV.

Table 1 shows the results of comparing the r values from SACJ vs. SV and SAI vs. SV. All three animals show that the correlation coefficient from SACJ vs. SV is significantly stronger than it from SAI vs. SV.

Figure 5 shows the scatter plots between DSA (the absolute difference of the value between the SACJ and SAI) and the DT (the absolute difference of the tissue volume) with linear regression in all three animals (average $r^2 = 0.86$). From the equation (11) and (16), we know that the SAI takes the assumption about no tissue volume change for a given voxel between the two volumes which may not be valid. Figure 5 shows that as the tissue volume change increases, the difference between the measures of regional ventilation from SACJ and SAI increases linearly in all animals.

Table 1. Comparison of ventilation measures between SACJ and SAI in small cube ROIs with size 20 mm \times 20 mm \times 20 mm

Animal	Correlation pair (with SV)	Correlation with SV (r value)	Number of samples	p value
A	SACJ	0.88	83	p \leq 0.0001
	SAI	0.65		
B	SACJ	0.93	119	p \leq 1.18e $^{-6}$
	SAI	0.77		
C	SACJ	0.89	86	p \leq 0.015
	SAI	0.78		

4 Discussion

We have described two measures to estimate regional ventilation from tissue volume and vesselness preserving image registration of CT images. The validity

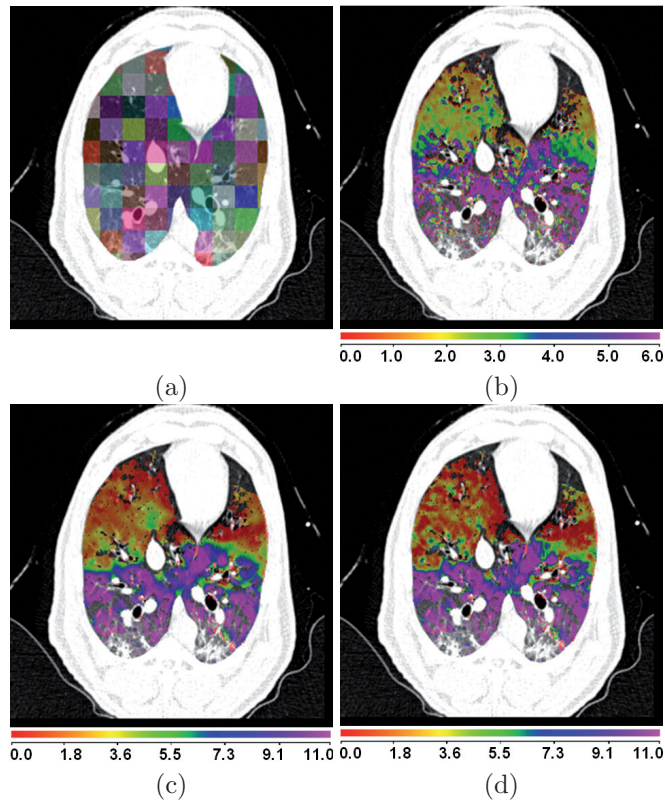


Fig. 3. (a): EE with color coded cubes showing the sample region. (b), (c), and (d): color map of the SV, SACJ and SAI.

and comparison of different measures for estimates of regional ventilation are evaluated by Xe-CT estimated ventilation. Individual regional ventilation measures are compared to Xe-CT estimates of ventilation by transforming them to the same coordinate system. The difference between two registration measures and their relationship with the tissue volume difference is analyzed using linear regression.

The tissue volume and vesselness preserving algorithm is used to register the EI to the EE for estimating ventilation measures. It is also used to register the EE_0 to the EE for comparing two ventilation measures to the Xe-CT based SV. About 200 anatomical landmarks are identified and annotated to evaluate the registration accuracy. The average landmark error is on the order of 1 mm after registration.

The ventilation measures SACJ and SAI are derived and the relationship between them is described. The SACJ is based on the voxel air-tissue fraction theory of HU. With further assumption about no change in the tissue volume between the corresponding voxels in the template and target images, SAI can be

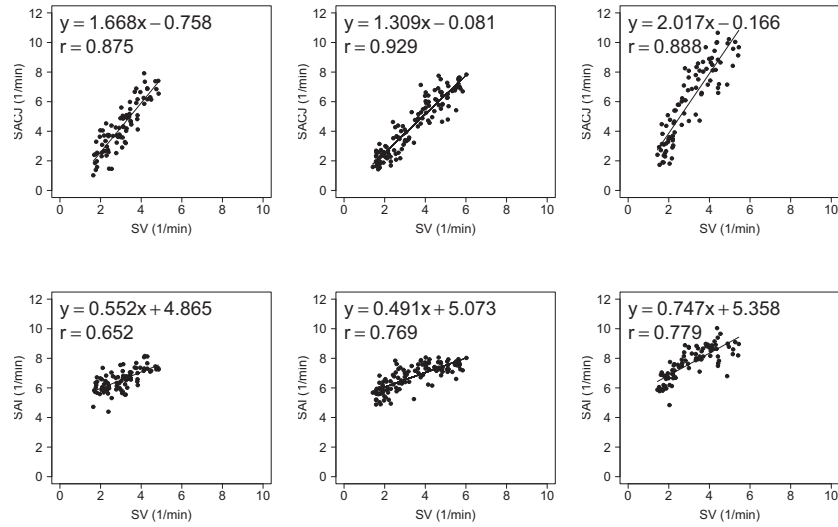


Fig. 4. Small cube ROIs with size 20 mm \times 20 mm \times 20 mm results for registration estimated ventilation measures compared to the Xe-CT estimated ventilation SV in scatter plot with linear regression in animals A, B, and C.

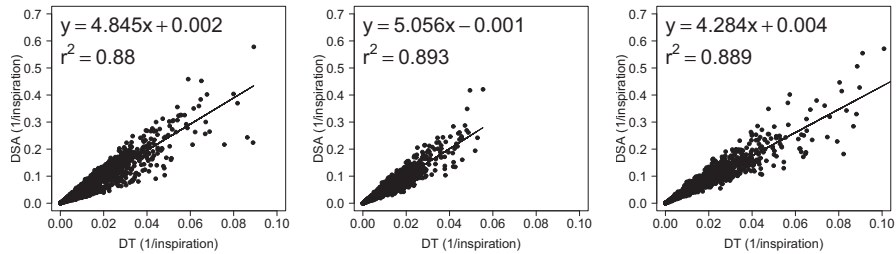


Fig. 5. (a) to (c): DSA (the absolute difference of the value between the SACJ and SAI) compared to DT (the absolute difference of the tissue volume) in animals A, B, and C.

calculated. Compared to SACJ which explicitly combines information both from the Jacobian and the intensity, SAI only uses the intensity information. SACJ has the most basic form for regional ventilation measure directly from the HU based voxel air-tissue fraction.

The two registration-based ventilation measures as well as the SV from Xe-CT are averaged and compared in predefined cubes. Averaging and comparing by 20 mm \times 20 mm \times 20 mm ROIs, the SACJ shows significantly higher correlation with Xe-CT based SV than the SAI in all three animals. By examining the

relationship between the DSA and DT, we see that the difference between SACJ and SAI may be due to the assumption of no tissue volume change (14) implicit in SAI. As the derivation in equations (11) and (16), to use SAI, the tissue volume change should be approximately zero. From Fig. 5, it is shown that while the tissue volume difference is usually small (less than 5%), regional ventilation measure SAI with the zero tissue volume change may introduce difference of more than 10% unit volume per inspiration comparing with the SACJ measure. For the ventilation measured over a minute, the DSA is about more than 1.7 unit volume per voxel (average $RR = 17.59$ breaths/min). Table 1 shows that the both the SACJ have significantly better correlation with SV than the SAI. This is consistent with the findings by Kabus et al. [4] who show that the Jacobian based ventilation has less error than the intensity based ventilation analysis using the segmented total lung volume as a global comparison.

The image registration algorithm used to find the transformation from EI to EE for measurement of regional ventilation produces accurate registrations by minimizing the tissue volume and vesselness measure difference between the template image and the target image. It would be interesting to compare different image registration algorithms and their effects on the registration-based ventilation measures. For example, if two registration algorithms achieve the similar landmark accuracy, the one does not preserve tissue volume change may show even larger difference in the SACJ and SAI measures than the results using TVP as described above.

In conclusion, with the same deformation field by the same image registration algorithm, a significant difference between the Jacobian based ventilation measures and the intensity based ventilation measure is found in a regional level using Xe-CT based ventilation measure SV. The ventilation measure by corrected Jacobian SACJ gives best correlation with Xe-CT based SV and the correlation is significantly higher than from the ventilation by intensity SAI indicating the ventilation measure by corrected Jacobian SACJ may be a better measure of regional lung ventilation from image registration of 4DCT images.

References

1. Guerrero, T., Sanders, K., Noyola-Martinez, J., Castillo, E., Zhang, Y., Tapia, R., Guerra, R., Borghero, Y., Komaki, R.: Quantification of regional ventilation from treatment planning CT. *International Journal of Radiation Oncology*Biophysics* **62**(3) (2005) 630 – 634
2. Reinhardt, J.M., Ding, K., Cao, K., Christensen, G.E., Hoffman, E.A., Bodas, S.V.: Registration-based estimates of local lung tissue expansion compared to xenon CT measures of specific ventilation. *Medical Image Analysis* **12**(6) (2008) 752 – 763 Special issue on information processing in medical imaging 2007.
3. Ding, K., Cao, K., Christensen, G.E., Hoffman, E.A., Reinhardt, J.M.: Registration-based regional lung mechanical analysis: Retrospectively reconstructed dynamic imaging versus static breath-hold image acquisition. Volume 7262., *SPIE* (2009) 72620D

4. Kabus, S., von Berg, J., Yamamoto, T., Opfer, R., Keall, P.J.: Lung ventilation estimation based on 4D-CT imaging. In: First International Workshop on Pulmonary Image Analysis, New York (2008) 73–81
5. Ding, K., Yin, Y., Cao, K., Christensen, G.E., Lin, C.L., Hoffman, E.A., Reinhardt, J.M.: Evaluation of lobar biomechanics during respiration using image registration. In: Proc. of International Conference on Medical Image Computing and Computer-Assisted Intervention 2009. Volume 5761. (2009) 739–746
6. Yaremko, B.P., Guerrero, T.M., Noyola-Martinez, J., Guerra, R., Lege, D.G., Nguyen, L.T., Balter, P.A., Cox, J.D., Komaki, R.: Reduction of normal lung irradiation in locally advanced non-small-cell lung cancer patients, using ventilation images for functional avoidance. *International Journal of Radiation Oncology*Biography*Physics* **68**(2) (2007) 562 – 571
7. Ding, K., Bayouth, J.E., Buatti, J.M., Christensen, G.E., Reinhardt, J.M.: 4dct-based measurement of changes in pulmonary function following a course of radiation therapy. *Medical Physics* **37**(3) (2010) 1261–1272
8. Chon, D., Simon, B.A., Beck, K.C., Shikata, H., Saba, O.I., Won, C., Hoffman, E.A.: Differences in regional wash-in and wash-out time constants for xenon-CT ventilation studies. *Respiratory Physiology & Neurobiology* **148**(1-2) (2005) 65 – 83
9. Yin, Y., Hoffman, E.A., Lin, C.L.: Mass preserving nonrigid registration of CT lung images using cubic B-spline. *Medical Physics* **36**(9) (2009) 4213–4222
10. Cao, K., Ding, K., Christensen, G.E., Reinhardt, J.M.: Tissue volume and vesselness measure preserving nonrigid registration of lung ct images. Volume 7623, SPIE (2010) 762309
11. Cao, K., Ding, K., Christensen, G.E., Raghavan, M.L., Amelon, R.E., Reinhardt, J.M.: Unifying Vascular Information in Intensity-Based Nonrigid Lung CT Registration. In Fischer, B., Dawant, B., Lorenz, C., eds.: *Biomedical Image Registration*, Lubeck (2010) 1–12
12. Hoffman, E.A., Ritman, E.L.: Effect of body orientation on regional lung expansion in dog and sloth. *J Appl Physiol* **59**(2) (1985) 481–491
13. Frangi, A.F., Niessen, W.J., Vincken, K.L., Viergever, M.A.: Multiscale vessel enhancement filtering. In: MICCAI. Volume 1496. (1998) 130–137
14. Choi, Y., Lee, S.: Injectivity conditions of 2d and 3d uniform cubic b-spline functions. *Graphical Models* **62**(6) (2000) 411–427
15. Simon, B.A.: Non-invasive imaging of regional lung function using X-Ray computed tomography. *Journal of Clinical Monitoring and Computing* **16**(5) (2000) 433 – 442
16. Fuld, M.K., Easley, R.B., Saba, O.I., Chon, D., Reinhardt, J.M., Hoffman, E.A., Simon, B.A.: CT-measured regional specific volume change reflects regional ventilation in supine sheep. *J Appl Physiol* **104**(4) (2008) 1177–1184
17. Guo, J., Fuld, M.K., Alford, S.K., Reinhardt, J.M., Hoffman, E.A.: Pulmonary analysis software suite 9.0: Integrating quantitative measures of function with structural analyses. In: First International Workshop on Pulmonary Image Analysis, New York (2008) 283–292
18. Murphy, K., van Ginneken, B., Pluim, J., Klein, S., Staring, M.: Semi-automatic reference standard construction for quantitative evaluation of lung CT registration. In: Proc. of International Conference on Medical Image Computing and Computer-Assisted Intervention 2008. Volume 5242. (2008) 1006–1013
19. Papoullis, A., ed.: *Probability and Statistics*. Prentence Hall, Englewood Cliffs, NJ (1990)